Visible Integral-field Replicable Unit Spectrograph (VIRUS) optical tolerance

Lee, Hanshin, Hill, Gary, Marshall, Jennifer, Vattiat, Brian, DePoy, Darren

Hanshin Lee, Gary J. Hill, Jennifer L. Marshall, Brian L. Vattiat, Darren L. DePoy, "Visible Integral-field Replicable Unit Spectrograph (VIRUS) optical tolerance," Proc. SPIE 7735, Ground-based and Airborne Instrumentation for Astronomy III, 77353X (20 July 2010); doi: 10.1117/12.857184

SPIE.

Event: SPIE Astronomical Telescopes + Instrumentation, 2010, San Diego, California, United States

Visible Integral-field Replicable Unit Spectrograph (VIRUS) Optical Tolerance

Hanshin Lee [a,*], Gary J. Hill[a], Jennifer L. Marshall[b], Brian L. Vattiat[a], Darren L. DePoy[b]
[a]McDonald Observatory, University of Texas at Austin, 1 University Station C1402, Austin, TX 78712-0259, USA;
[b]Department of Physics and Astronomy, Texas A&M University, 4242 TAMU, College Station, TX 77843-4242, USA

ABSTRACT

The Visible Integral-field Replicable Unit Spectrograph (VIRUS) instrument is made up of 150+ individually compact and identical spectrographs, each fed by a fiber integral field unit. The instrument provides integral field spectroscopy from 350 nm to 550 nm of over 33,600 spatial elements per observation, each 1.8 arcsec^2 on the sky, at R ~ 700. The instrument will be fed by a new wide-field corrector (WFC) of the Hobby-Eberly Telescope (HET[†]) with increased science field of view as large as 22 arcmin diameter and telescope aperture of 10 m. The construction of the large number of VIRUS units requires the individual spectrographs be interchangeable at sub-system level and a production line assembly process be utilized, while meeting the optical performance specification. These requirements pose a strong emphasis on careful analysis of the manufacturing and alignment tolerances of the unit spectrograph design. In this paper, we detail the tolerance analysis, and discuss its implication to the optical performance and production of the VIRUS instrument.

Keywords: VIRUS, Optical tolerance, Hobby-Eberly Telescope, HETDEX

1. INTRODUCTION: HETDEX, WIDE FIELD UPGRADE, AND VIRUS INSTRUMENT

The main science motivation of the VIRUS instrument [1] is to map the evolution of dark energy for the Hobby-Eberly Telescope Dark Energy Experiment (HETDEX) [2], by observing 0.8M Lyman-α emitting galaxies as tracers. In order to achieve this science objective, we are conducting three main engineering/science projects: a major telescope upgrade including replacing the top end of the telescope to allow for a larger focal plane (Wide Field Upgrade)[3], the construction of the Visual Integral-Field Replicable Unit Spectrograph (VIRUS) instrument, and the execution of a large area (5000 square degrees) blind survey for Lyman-α emitting galaxies at redshifts $z < 3.5$.

The requirement to survey large areas of sky with VIRUS and the need to perform wavefront sensing for closed-loop active alignment control of the tracker position led us to design a new corrector employing meter-scale mirrors and covering a 22-arcmin diameter field of view. The HET Wide Field Upgrade (WFU) deploys this wide field corrector (WFC), a new tracker prime focus instrument package (PFIP), and new metrology systems. The new corrector has improved image quality and a 10 m pupil diameter. The periphery of the field will be used for guiding and wavefront sensing to provide the necessary feedback to maintain the telescope alignment correctly. The WFC will give 30 times larger observing area than the current HET corrector. It is a four-mirror design with two concave 1 meter diameter mirrors, one concave 0.9 meter diameter mirror, and one convex 0.23 m diameter mirror. In order to feed optical fibers at f/3.65 to minimize focal ratio degradation (FRD), the WFC is designed to be telecentric at its curved focal surface so that the chief rays from all field angles are normal to the concave spherical focal surface centered at the exit pupil vertex. Due to excellent aberration correction, the imaging performance of the WFC is 0.5arcsec or better over the entire field of view with minimal obscuration across the field. The College of Optical Sciences at the University of Arizona is manufacturing the WFC[4]. A new tracker is needed to accommodate the size and four-fold weight increase of the new PFIP. It will be a third generation evolution of the trackers for HET and SALT, and is in essence a precision six-axis

* Hanshin Lee E-mail: lee@astro.as.utexas.edu

† The Hobby – Eberly Telescope is operated by McDonald Observatory on behalf of the University of Texas at Austin, the Pennsylvania State University, Stanford University, Ludwig-Maximillians-Universität München, and Georg-August-Universität, Göttingen.

Ground-based and Airborne Instrumentation for Astronomy III, edited by Ian S. McLean, Suzanne K. Ramsay, Hideki Takami, Proc. of SPIE Vol. 7735, 77353X · © 2010 SPIE · CCC code: 0277-786X/10/$18 · doi: 10.1117/12.857184

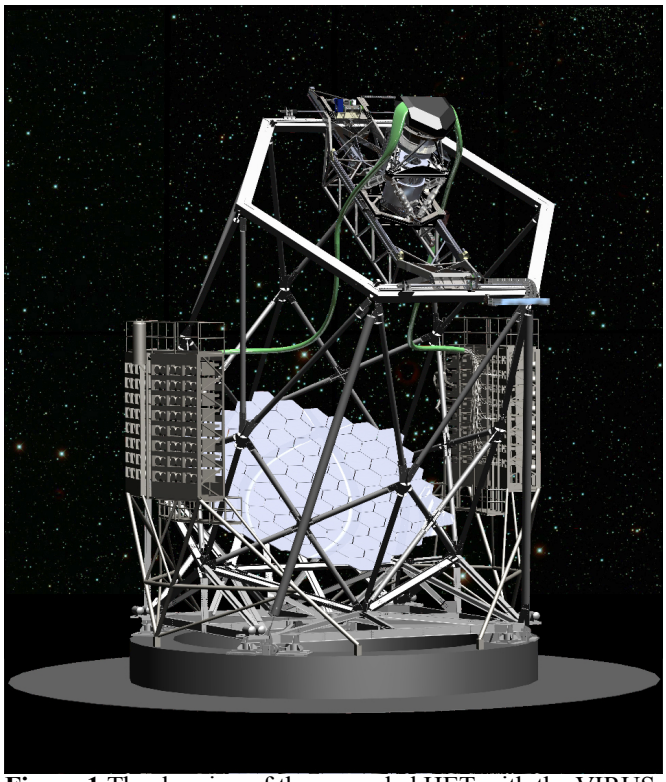

Figure 1 The drawing of the upgraded HET with the VIRUS instrument mounted on the telescope.

motion control stage. The tracker is being developed by the Center for Electro-Mechanics (CEM) at the University of Texas at Austin, with integration at the CEM facility scheduled for Fall 2010.

VIRUS is based upon a novel instrument design philosophy unlike that used in traditional astronomical spectroscopic instrumentation where a monolithic single spectrograph for a large telescope with large and expensive optics and mechanisms observes a contiguous region on the focal plane of the telescope. We have taken a different approach to designing the VIRUS instrument based on our concept and studies[5-8], where we concluded that industrial replication offers significant cost-advantages when compared to a traditional monolithic spectrograph, particularly in the cost of the optics and engineering effort. This concept appears to be a cost-effective approach to outfitting existing large telescopes as well as the coming generation of ELTs, for certain instrument types, where the multiplex advantage can be used to image-slice and thus avoid growth in the scale of instruments with telescope aperture. This new approach led us to the VIRUS instrument design as follows. The entire VIRUS instrument is comprised of an array of simple, compact, inexpensive, and yet highly performing unit optical spectrographs. Each VIRUS unit contains two spectrograph channels and samples only a small fraction of the telescope focal plane that is finely sampled by 448 fibers each covering 1.8arcsec^2 on the sky. The fibers feeding a two-channel unit module are hexagonal-close-packaged in a square array format that covers a 50×50arcsec^2 Integral Field Unit (IFU) with a 1/3 fill-factor. A three-exposure dither pattern fills in the gap. The optics of the unit spectrograph is essentially based upon a two Schmidt design; one as a collimator in a reversed Schmidt form and the other as a camera in a normal Schmidt design, both joined together at a common pupil plane. The optical beam train is formed by three reflections and four refractions (i.e. three mirrors and two lenses). With dielectric reflective coatings optimized for the wavelength range, high throughput is obtained. The full VIRUS array will consist of between 150 and 194 channels, depending on funding, and will simultaneously observe a minimum of 33,600 spectra with 12 million resolution elements. The IFUs are arrayed within the 22′ field of the upgraded HET with ~1/7 fill factor, sufficient to detect the required density of LAEs for HETDEX. Development is proceeding with the prototype (VIRUS-P [8]), deployed in October 2006, and the production prototype where value engineering has been used to reduce the cost for production. Figure 1 shows a rendering of the upgraded telescope, showing VIRUS mounted on the telescope.

The construction of the large number of VIRUS units requires the individual spectrographs be interchangeable at the sub-system level and a production line assembly process be utilized, while meeting the optical performance specification [9]. These requirements pose a strong emphasis on careful analysis of the manufacturing and alignment tolerances of the unit spectrograph design. In this paper, we detail the tolerance analysis, and discuss its implication to the optical performance and production of the VIRUS instrument.

2. OPTICAL DESIGN AND TOLERANCE OF VIRUS SPECTROGRAPH

2.1 Overview

Figure 2 illustrates the optical layout of a single channel of the VIRUS unit and a sectioned view of the two-channel VIRUS unit opto-mechanical model. The optical design of the spectrograph is comprised of two sub-systems, both based upon the Schmidt design concept. The first sub-system is the collimator that consists of the entrance slit of 224 fibers, a collimation mirror, and a folding flat mirror. The entrance slit is curved with a curvature twice that of the collimator mirror to form the pupil for all fibers at a distance from the vertex of the collimation mirror roughly equal to the radius

of curvature of the collimation mirror, making the collimator essentially a reversed Schmidt design without an aspheric corrector plate. The fiber slit is bonded to a cylindrical lens which heals residual surface roughness to controls the fiber focal ratio degradation (FRD). Although f/3.65 is the nominal input and exit focal ratio, the optical components are slightly oversized to be able to accept f/3.33 to accommodate a small amount of FRD and angular misalignments in manufacture of the fiber cables [10]. The folding flat mirror then transfers the pupil to the position of the grating, roughly in line with the collimation mirror, in order to make the design compact and to minimize obstruction by the input slit assembly which sits in a relieved slot in the back of the fold flat.

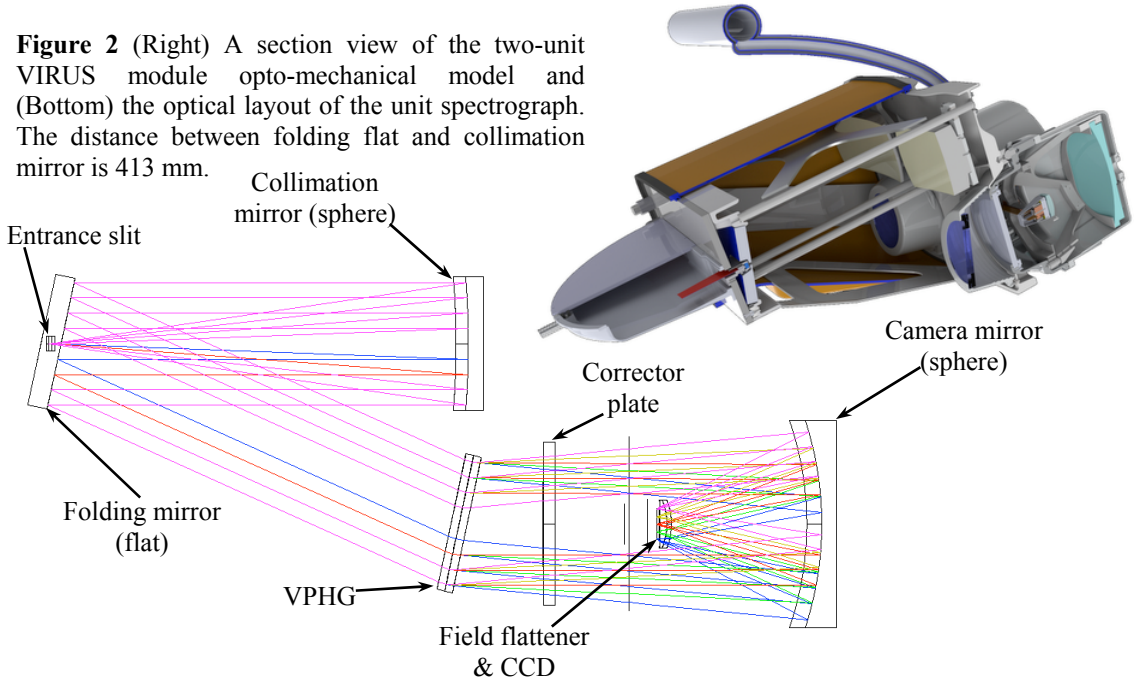

Figure 2 (Right) A section view of the two-unit VIRUS module opto-mechanical model and (Bottom) the optical layout of the unit spectrograph. The distance between folding flat and collimation mirror is 413 mm.

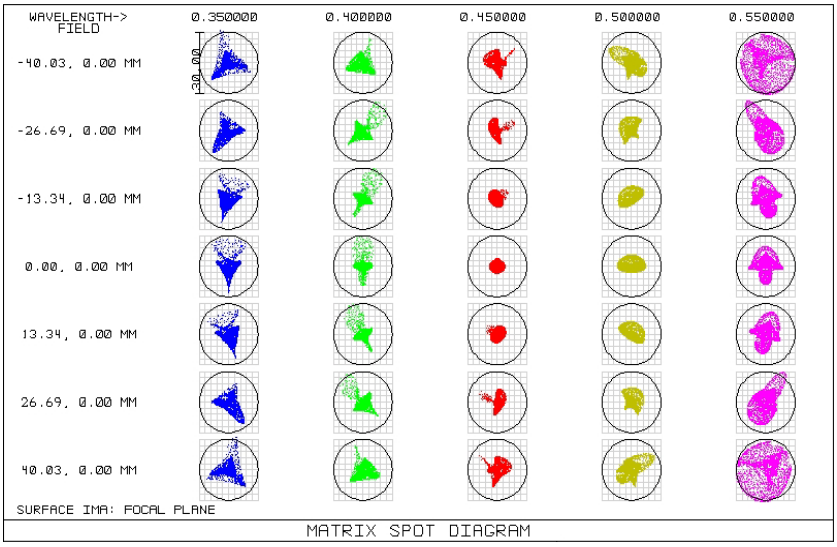

Figure 3 A matrix spot diagram of the VIRUS unit spectrograph. The circles are 30 μm in diameter.

At the pupil, a Volume Phase Holographic Grating (VPHG[11]) is located to disperse the beam into spectral elements. At the beam angle of incidence of 12.15 deg with respect to the grating normal, the 930 lines/mm VPHG gives R = 700 with coverage optimized for 350-550 nm. The dispersed beam then propagates through the camera sub-system that is essentially a Schmidt camera. The corrector plate, with an even aspheric surface profile on the front surface, overcorrects the system spherical aberration of both the camera and collimator, which is then optimally balanced by the spherical f/1.25 camera mirror. The undesired feature of a Schmidt camera is a curved focal surface that is flattened by the convex spherical front surface of the field flattener. Residual aberrations are further corrected by the even aspheric back surface of the field flattener. The camera is evacuated and has the CCD mounted internally at the focus. The spectrograph optical design focal reduces the f/3.33 beam into f/1.25 at the camera focal plane, a linear demagnification of 2.66, yielding 1 resolution element size of roughly 100 μm at the CCD for the

266 μm core size of the fiber. The mechanical section view in Figure 2 shows the IFU slit sub-assembly mounted to the collimator sub-assembly on the left, and the camera sub-assembly mounted on the right[12]. The CCD is cooled by a flexible line from above with a breakable cryogenic bayonet connection[13]. The spot diagram of the VIRUS unit spectrograph is shown in Figure 3. The practical implementation of the VIRUS optical design is informed by the prototype VIRUS-P that has been in operation at the McDonald Observatory since late 2006[8]. The prototype proved the optical design will meet requirements and has allowed the opto-mechanical design to be tested end-to-end in real operations. VIRUS-P has also allowed the development of software pipelines that are directly scalable to the final VIRUS [1].

2.2 Tolerance analysis

For budgeting realistic optical tolerances of the unit spectrograph, we made an effort to reflect important opto-mechanical assembly plans and/or requirements into the tolerance analysis as much as possible. One of the critical design requirements, which needs be considered in the tolerance analysis, is that the camera units be interchangeable amongst any collimator unit once the instrument is on the telescope. This requirement will make it possible to swap cameras during operations, minimizing down time of the instrument in the case of readout electronics or vacuum. In order to meet the sub-system interchangeability requirement, we plan to align each VIRUS collimator pair with a "fiducial" camera and align each camera with a "fiducial" collimator. These fiducial units will be mechanically and optically identical to the other VIRUS units, and will provide a constant reference for the optical alignment amongst all 150+ VIRUS spectrographs[9].

Because the collimator is much simpler to set up than the camera, we will build the fiducial collimator first. A calibrated commercial telescope or camera can be used as a fiducial camera for the collimator build. Alignment of the collimator will follow the scheme established for VIRUS-P, using a laser to establish each of the optical axes in the pair of channels [8]. The kinematic mount for the fiber slit assembly acts as the reference for the optical axes and a fiducial fiber will be the reference for each channel. Tip/tilt/decenter error can be well constrained during this process. For constraining defocus error, we plan to use a wavefront sensor. The sensor can be attached at the focus of the fiducial camera looking through the collimator. The sensed collimator aberrations can be analyzed to find the optimum focus adjustment of the collimator mirror. These alignment procedures result in the fiducial collimator. The fiducial camera is then aligned with respect to this fiducial collimator. It is not desirable to attempt to precisely align every single optical element with respect to some reference. Rather, we can manufacture and assemble some of the optical components with relaxed tolerance, achieved with machine level precision, while having a compensation component to nullify any degradation in image quality and/or image position/size due to the loose-tolerance elements as much as possible. Given the fact that the collimator and camera sub-systems can be separately aligned with respect to a reference fiducial system, we can have a separate compensation component in the individual subsystems. The natural compensation elements are the collimation mirror and camera mirror for the collimator and camera, respectively. The elements are adjustable in tip, tilt, and focus in the tolerance analysis.

For the tolerance analysis, we have used two merits. One is that the full-width-half-maximum (FWHM) of the point spread function (PSF) shall be smaller than 2 pixels (30μm) across 95% of the area of the focal surface. The other is that the centroid of the image shall be misplaced by no more than the size of 1 resolution element (~100μm). Keeping these two merits within the requirements enables us to keep the correct spectral resolution with a high SNR, to minimize cross-talk between adjacent fibers, and to capture the nominal number of resolution elements from a single spectral image. The image quality specification is driven by the need to separate the spectra from adjacent fibers, rather than as a percentage degradation of the image size of a single fiber. Some examples of how the image quality degradation of the spectrograph (in terms of FWHM) can affect the spectral lines are shown in Figure 4. As the FWHM increases from 0.05pixel to 2 pixel, the image of three adjacent resolution elements (with equal flux) appears to show significant spread (Column A) while the spread in the integrated profile (Column B) is less significant. This means that the two dimensional image quality requirement given in terms of the FWHM of a 2D PSF could be further relaxed because the quantity that we actually care about is a spectral profile rather than 2D spectra. However, it was observed that significant flux from adjacent fiber images quickly spread into the inter-fiber gaps (that are supposed to be dark enough to distinguish adjacent spectra) on the CCD with FWHM larger than 2.3 pixels. 2.0 pixels FWHM for the point spread function appears to be the appropriate image quality requirement for the analysis.

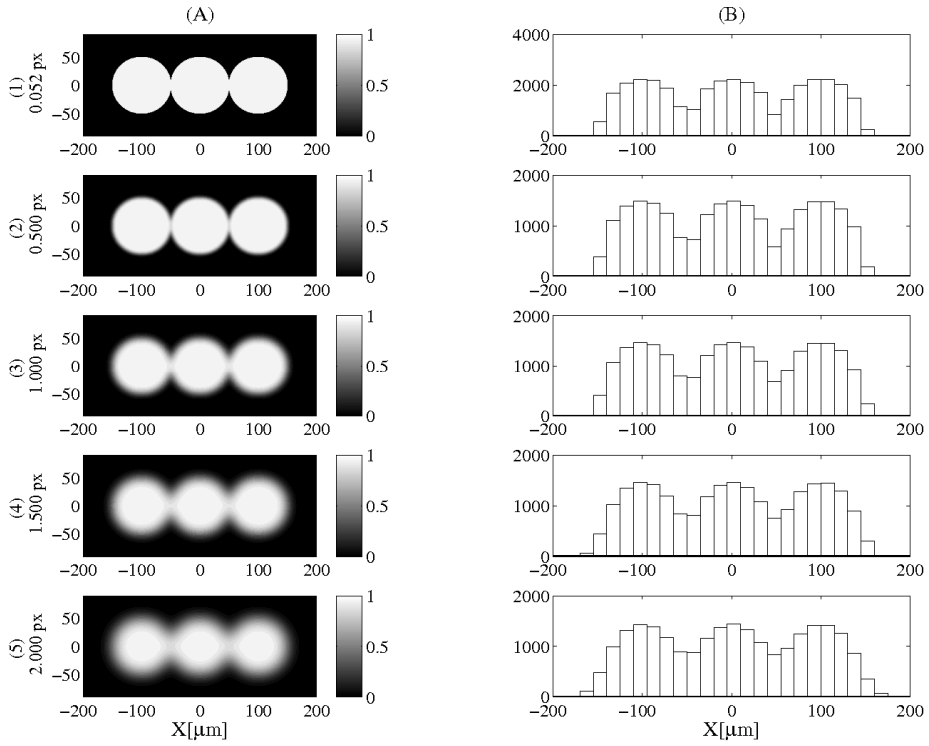

Figure 4 (Column A) A simulated image of three adjacent fiber resolution elements with the same flux. (Column B) The pixelated spectral profile of the spectra (i.e. integrated along the vertical direction). (From row 1 to 5) images and profiles with different FWHM of the Gaussian PSF of the spectrograph. Note that the color scale on the left column and the vertical scale on the right column are arbitrary.

At the start, the sensitivities of individual tolerance parameters were explored and these were summed in quadrature in order to see the expected variations in the merits and to make a rough error budget for the tolerance parameters. In so doing, individual tolerance parameters were either relaxed or tightened based on the impact of individual parameters on the merits. This process was iterated until the variations in the merits become close to the requirement, leading to the first estimate of the tolerance error budget. Note that the compensators were adjusted during the sensitivity calculations without any restriction in adjustment range and resolution.

The individual tolerance parameters were then randomly perturbed within the ranges specified in the first tolerance error budget from the sensitivity analysis. A uniform distribution was used for generating the random perturbation as it gives more conservative estimates than a Gaussian. Monte-Carlo (MC) tolerance analysis can reveal more realistic impacts of individual tolerance parameters on the merits. In the sensitivity analysis, it was assumed that the individual tolerance parameters are statistically independent, thus ignoring coupling effects between the parameters. In contrast, the MC analysis is based on exact ray-tracing, thus completely taking into account such coupling effects. In fact the MC analysis indicated the existence of a few coupling effects between parameters and that the first error budget table actually underestimated the error budget, i.e. the sensitivity-based error budget led to much larger variations in the merits than what was predicted with the variables independent from each other. Therefore, it was necessary to iterate the MC analysis by adjusting the error budgets of the tolerance parameters. The stopping criterion of this iteration could be arbitrary. For a one-off realization as in conventional instrumentation, the stopping criterion can be something like "*until 100% of N random realizations in the MC analysis meet the optical tolerance criteria*". In our case where we are building 150+ identical spectrographs, imposing the stopping criterion in the same way is likely to lead to rather tight manufacturing and alignment error budgets, and thus to higher cost and longer delivery schedule than anticipated and desired. Thus, we allowed 10% of random realizations of the VIRUS unit spectrograph to be beyond the boundary set by the criteria. Note that although 10% of the realizations do not meet the image quality criterion, the PSF FWHM over a significant portion of the CCD is still within specification. The MC analysis was iterated until this condition was met, leading to the final estimate of the tolerance error budget. During the MC analysis, two sets of populations of the camera and collimator systems with random perturbations were produced. Sets of VIRUS units were then created by combining

a camera and collimator randomly picked from the two pools. This approach takes care of the required interchangeability of cameras.

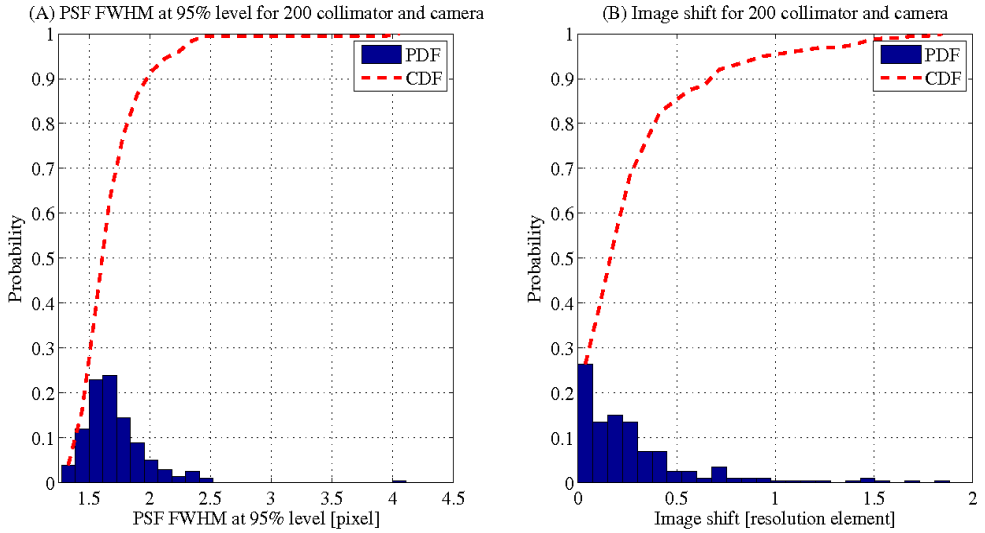

Figure 6 The distributions of the expected FWHM and Image shift of 200 random realizations of the VIRUS unit spectrograph based on the tolerance error budget in Table 1. The tolerance criteria: i) the full-width-half-maximum (FWHM) of the point spread function (PSF) shall be smaller than 2 pixels (30 μm) across 95% of the area of the focal surface. ii) the centroid of the image shall be misplaced by no more than the size of 1 resolution element (~100 μm).

Figure 6 shows the expected distributions of the image quality and image shift of 200 VIRUS unit spectrographs based on the alignment and manufacturing tolerances given in Table 1. The compensation ranges are ±1 mm in focus and ±0.3 ° in tip/tilt for both spherical mirror compensators. The assumed compensation resolution of 10 μm in focus and 10 arcsec in tip/tilt appears to be adequate. These parameters have been adopted for the production VIRUS optics and mechanical design.

Table 1 The optical tolerance for manufacturing and alignment of VIRUS unit spectrograph (COMP: compensator).

Element	Wedge / centration / thickness			Radius	Figure (wv=632.8nm)	Index / dispersion		Alignment (decenter/tip/focus)		
Slit lens	0.1°	0.1 mm	0.1 mm	1 mm	1 wv [p-p]	1%	1%	0.1 mm	0.1°	0.1 mm
Collimator mirror	--	--	--	0.5 mm	1/4 wv [rms]	--	--	COMP	COMP	COMP
Folding flat mirror	--	--	--	--	1 wv [p-p]	--	--	--	0.1°	0.1 mm
VPHG (930±2 l/mm)	0.1°	--	0.1 mm	--	1 wv [p-p]	1%	1%	0.1 mm	0.1°	0.1 mm
Corrector	0.1°	0.1 mm	0.1 mm	--	1 wv [p-p] - RMS MSFE 16 nm Scale 1 mm~20 mm - RMS roughness 2 nm scale < 1 mm	1%	1%	0.1 mm	0.05°	0.1 mm
Camera mirror	--	--	--	0.5 mm	1/8 wv [rms]	--	--	COMP	COMP	COMP
Field flattener	0.1°	0.1 mm	0.05 mm	0.1 mm	1 wv [p-p] - RMS MSFE 16 nm Scale 0.2 mm~3 mm - RMS roughness 2 nm(scale < 0.2 mm)	1%	1%	0.1 mm (w.r.t. CCD)	0.05° (w.r.t. CCD)	0.05 mm (w.r.t. CCD)
CCD	--	--	--	--	31 wv [p-p]	--	--	--	--	--
Camera subsystem	--	--	--	--	--	--	--	0.1 mm (w.r.t. Collimator)	0.05° (w.r.t. Collimator)	0.1 mm (w.r.t. Collimator)

2.3 Mid-spatial frequency surface error (MSFE)

The corrector plate and field flattener each contain even aspheric profiles on one flat surface to balance spherical aberration from the collimator and camera mirrors (corrector plate) and to correct residual aberrations (field flattener). In addition to other tolerances like the surface figure error requirement, the mid-spatial frequency error (MSFE) specifications also need to be defined for these surfaces. Unlike full-aperture tools used in generating spherically figured surfaces, the asphere figuring process uses sub-aperture tools. As a result, aspheric surfaces are more likely to contain significant residual periodic surface (radial) profiles left by a combination of tool path errors of different sub-aperture tools used in the figuring process. These residual structures have mid-spatial frequencies that are higher than what low-spatial frequency figure errors (LSFE. e.g. the first 37 Zernike terms) normally have, but lower than what high-spatial frequency surface errors (HSFE, i.e. roughness) usually have. In terms of image formation, LSFE results in a fatter PSF, while retaining the peak and nodes of the PSF. HSFE essentially scatters energy far away from the main PSF central peak thus is treated as a scattering loss without affecting the FWHM of the PSF significantly. Between these two limits, MSFE causes erosion of the PSF peak and nodes, resulting in spread of energy of a resolution element into adjacent ones, thus making it more difficult to resolve adjacent spectral resolution elements. Here, we wish to have loss no more than 10% of the energy from the nominal PSF due to the mid-spatial frequency error.

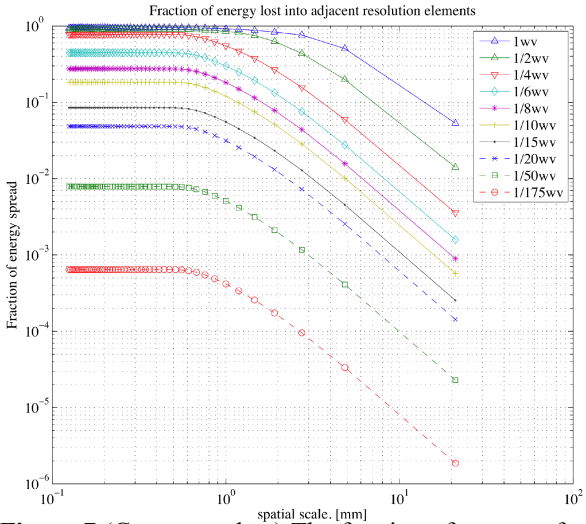

Figure 7 (Corrector plate) The fraction of energy of a resolution element lost into its neighbor at different spatial scales with different amplitudes of sinusoidal wavefront deformation. (wv = 350 nm)

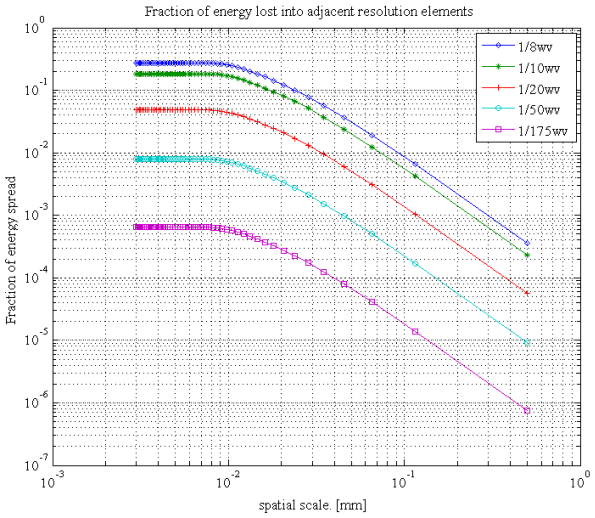

Figure 8 (Field flattener) The fraction of energy of a resolution element lost into its neighbor at different spatial scales with different amplitudes of sinusoidal wavefront deformation. (wv=350 nm)

For the corrector plate (Figure 7), the spatial scale of interest is between 1 mm and 20 mm. We regard scales below 1 mm as surface roughness for the purposes of this analysis. Figure 7 shows the fraction of energy lost from a spectral resolution element into its neighbor as a function of spatial scale with different amplitudes of sinusoidal wavefront deformation. At the minimum spatial scale, the curves generally develop a plateau, meaning that the beam angle at these scales is much wider than what is subtended by a single resolution element. Thus, these should be treated as a scattering loss. Assuming typical 2 nm rms surface roughness for all optical surfaces, the total rms wavefront deformation below the minimum scale is 7.4 nm (i.e. 1/33 wave in amplitude). This leads to about a couple of percent loss by the surface roughness. On the other hand, the curves consistently decrease at spatial scales longer than 1 mm. To ensure less than a 10% loss of light from the PSF on this mid-spatial scale, we set the maximum amplitude of wavefront deformation to be less than 1/10 wave. Thus, each surface can have 8 nm rms in wavefront deformation due to MSFE. For the corrector plate, this translates to MSFE of 16.5 nm (1/20 wave) rms.

For the field flattener (Figure 8), the beam footprint on the aspheric surface is only 3mm in diameter. This is much smaller than that of the corrector plate. However, it is close to the CCD (2.5 mm separation). We can approximate this element as a separate system where the pupil has 3 mm diameter and the focal length is 2.5 mm (f/0.8), because what we care about are spatial scales of MSFE smaller than the beam footprint. In this case, the energy loss curves gradually develop a plateau at 0.02 mm, so we treat this as the minimum of the MSFE of the field flattener. Again, 2 nm rms below this minimum spatial scale would contribute less than a few fraction of percent loss to the total. MSFE of 1/20

wave rms at spatial scales between 0.02 mm and 3 mm appears to be adequate for the field flattener. However, surface errors at spatial scale smaller than 0.2mm are more like surface roughness, so we set the minimum scale to 0.2mm for the field flattener. It is reported that spherical surfaces made by conventional polishing processes consistently show far less than 6 nm rms of residual MSFE at spatial scales between 0.1mm and 6.5mm while, for deterministic sub-aperture tool polishing processes, the MSFE in the same spatial scale range is between 6 nm and 18 nm[14-15]. Our MSFE tolerances appear to be consistent with these observed values in practice.

3. SUMMARY

In this paper, we discussed the optical tolerance analysis and error budgets of the VIRUS unit spectrograph. Unlike conventional one-off astronomical instruments, the construction of the large number of VIRUS units requires the individual spectrographs to be interchangeable at the sub-system level and a production line assembly process to be utilized, while meeting the optical performance specification. These requirements create a strong emphasis on careful analysis of the manufacturing and alignment tolerances of the unit spectrograph design and trade-offs between optical performance, delivery schedule, and cost. The final error budget of the VIRUS unit spectrograph implies that the manufacturing and alignment tolerances are adequately chosen to keep the optics manufacturing cost within our anticipated budget while making a straightforward assembly and test possible with minimal impact on the optical performance of the 200 unit spectrographs. In order to ensure the optical performance and further speed up the assembly and test process, we are exploring various testing methods for the VIRUS spectrograph alignment. One efficient method uses a wavefront sensor in the fiducial collimator alignment to measure low-order aberrations that will establish the required tip/tilt/focus compensation for the collimator channels. Against this fiducial collimator, the fiducial camera will be created and its alignment-test will be aided by software that analyzes through-focus CCD images to produce instruction for focus/tip/tilt compensation of the camera mirror. During these alignment processes, the folding flat and VPHG grating, the Schmidt corrector, and the field flattener remain fixed, having been positioned by manufacturing tolerances and external jigs. Once these fiducial systems are completed, the rest of the collimators (and cameras) are aligned with respect to the fiducial camera (and collimator). The same alignment procedures are to be iterated for the rest of the spectrographs. This alignment procedure will be quick, straightforward, and deterministic so that a technician with minimal optics background can align the optics. We are developing details of the wavefront sensor and image-based alignment tools. The new tracker will be assembled and tested at CEM at the end of 2010, allowing six months for characterization and software development. In parallel, the production of VIRUS will start at the end of 2010 with the first delivery of detectors. The assembly and test of VIRUS will take place at TAMU, where a production line is being set up[9]. A large newly outfitted lab space is being adapted to the production line. The assembly flow is being detailed down to the part level in preparation for assembling the first units in August 2010, and lessons learned from that exercise will be incorporated into the production assembly starting in early 2011. We are planning for deployment of the upgrade and VIRUS in about 12 months from the time of writing.

ACKNOWLEDGEMENTS

HETDEX is led by the University of Texas at Austin McDonald Observatory and Department of Astronomy with participation from the Universitäts-Sternwarte of the Ludwig-Maximilians-Universität München, the Max-Planck-Institut für Extraterrestriche-Physik (MPE), Astrophysikalisches Institut Potsdam (AIP), Texas A&M University, Pennsylvania State University, and the HET consortium. In addition to Institutional support, HETDEX is funded in part by gifts from Harold C. Simmons, Robert and Annie Graham, The Cynthia and George Mitchell Foundation, Louis and Julia Beecherl, Jim and Charlotte Finley, Bill and Bettye Nowlin, Robert and Fallon Vaughn, Eric Stumberg, and many others, by AFRL under agreement number FA9451-04-2-0355, and by the Texas Norman Hackerman Advanced Research Program under grants 003658-0005-2006 and 003658-0295-2007.

REFERENCES

[1] G.J. Hill, et al., "VIRUS: a massively replicated 33k fiber integral field spectrograph for the upgraded Hobby-Eberly Telescope," Proc. SPIE, **7735**-21 (2010)

[2] G. J. Hill, et al., "The Hobby-Eberly Telescope Dark Energy Experiment," AIP Conference Proceedings, **773** 224-223 (2004).
[3] R. Savage, et al., "Current Status of the Hobby-Eberly Telescope wide field upgrade," Proc. SPIE, **7733**-149 (2010).
[4] J. H. Burge, S. D. Benjamin, M. B. Dubin, S. M. Manuel, M. J. Novak, Chang Jin Oh, M. J. Valente, C. Zhao, J. A. Booth, J. M. Good, G. J. Hill, H. Lee, P. J. MacQueen, M. D. Rafal, R. D. Savage, M. P. Smith, B. L. Vattiat, "Development of a wide-field spherical aberration corrector for the Hobby Eberly Telescope", Proc. SPIE, **7733**-51 (2010).
[5] G.J. Hill, P.J. MacQueen, C. Tejada, P.J. Cobos, P. Palunas, K. Gebhardt, & N. Drory, "VIRUS: a massively replicated IFU spectrograph for HET," *Proc. SPIE*, **5492**, 25 (2004).
[6] G.J. Hill, P.J. MacQueen, P. Palunas, A. Kelz, M.M. Roth, K. Gebhardt, & F. Grupp, "VIRUS: a hugely replicated integral field spectrograph for HETDEX", *New Astronomy Reviews*, **50**, 378 (2006).
[7] G.J. Hill, P.J. MacQueen, J.R. Tufts, A. Kelz, M.M. Roth, W. Altmann, P. Segura, M. Smith, K. Gebhardt, & P. Palunas, "VIRUS: a massively-replicated IFU spectrograph for HET," *Proc. SPIE*, **6269**, paper 6269-93 (2006)
[8] G.J. Hill, P.J. MacQueen, M.P. Smith, J.R. Tufts, M.M. Roth, A. Kelz, J. J. Adams, N. Drory, S.I. Barnes, G.A. Blanc, J.D. Murphy, K. Gebhardt, W. Altmann, G.L. Wesley, P.R. Segura, J.M. Good, J.A. Booth, S.-M. Bauer, J.A. Goertz, R.D. Edmonston, C.P. Wilkinson, "Design, construction, and performance of VIRUS-P: the prototype of a highly replicated integral-field spectrograph for HET", *Proc. SPIE*, **7014**-257 (2008).
[9] J.L. Marshall, et al., "Production-line assembly of 150+ VIRUS spectrographs," Proc. SPIE, 7735-163 (2010).
[10] A. Kelz, et al., "Production and performance of replicable integral field units for VIRUS," Proc. SPIE, 7735-178 (2010).
[11] Barden, S. C., Arns, J. A., and Colburn, W. S., "Volume-phase holographic gratings and their potential for astronomical applications," Proc. SPIE **3355**, 866 (1998).
[12] B. Vattiat, et al., "Mechanical design evolution of the VIRUS instrument for volume production and deployment," Proc. SPIE, 7735-264 (2010).
[13] T.S. Chonis, et al., "Development of a cryogenic system for the VIRUS array of 150 spectrographs for the Hobby-Eberly Telescope," Proc. SPIE, 7735-265 (2010).
[14] David M. Aikens et al., "Specification and Control of Mid-Spatial Frequency Wavefront Errors in Optical Systems," OSA Optical Fabrication and Testing Conference Proceedings (2008).
[15] M. Shibuya et. al. "Classification of undulated wavefront aberration in projection optics by considering its physical effects", Optical Engineering 45(5), pp 053001-6 (2007).